



Analysis of a cryolava flow-like feature on Titan

L. Le Corre^{a,*}, S. Le Mouélic^a, C. Sotin^b, J.-P. Combe^c, S. Rodriguez^d, J.W. Barnes^e, R.H. Brown^f, B.J. Buratti^b, R. Jaumann^g, J. Soderblom^f, L.A. Soderblom^h, R. Clarkⁱ, K.H. Baines^b, P.D. Nicholson^j

^a CNRS, Université de Nantes, Laboratoire de Planétologie et Géodynamique, UMR 6112, 2 rue de la Houssinière, Nantes F-44000, France

^b Jet Propulsion Laboratory, Caltech, 4800 Oak Grove Drive, Pasadena, CA 91109, USA

^c Bear Fight Center, A Columbus Technologies and Services Inc. Affiliate, P.O. Box 667, 22 Fiddler's Road, Winthrop, WA 98862, USA

^d Laboratoire AIM, CEA Orme des Merisiers, DSM/IRFU/SAP, France

^e Department of Physics, University of Idaho Engineering-Physics Building, Moscow, ID 83844, USA

^f Department of Planetary Sciences, University of Arizona, Lunar and Planetary Laboratory, 1629 E. University Blvd., Tucson, AZ 85721-0092, USA

^g DLR, Institute of Planetary Research, Rutherfordstrasse 2, 12489 Berlin, Germany

^h United States Geological Survey, 2255 N. Gemini Drive, Flagstaff, AZ 86001, USA

ⁱ United States Geological Survey, Mail Stop 964, Box 25046, Denver Federal Center, Denver, CO 80225, USA

^j Department of Astronomy, Cornell University, 418 Space Sciences Building, Ithaca, NY 14853, USA

ARTICLE INFO

Article history:

Received 9 December 2008

Received in revised form

5 March 2009

Accepted 10 March 2009

Available online 18 March 2009

Keywords:

Infrared observations

Radar observations

Infrared spectroscopy

Titan

ABSTRACT

This paper reports on the analysis of the highest spatial resolution hyperspectral images acquired by the Visual and Infrared Mapping Spectrometer (VIMS) onboard the Cassini spacecraft during its prime mission. A bright area matches a flow-like feature coming out of a caldera-like feature observed in Synthetic Aperture Radar (SAR) data recorded by the Cassini radar experiment [Lopes et al., 2007. Cryovolcanic features on Titan's surface as revealed by the Cassini Titan Radar Mapper. *Icarus* 186, 395–412, doi:10.1016/j.icarus.2006.09.006]. In this SAR image, the flow extends about 160 km east of the caldera. The contrast in brightness between the flow and the surroundings progressively vanishes, suggesting alteration or evolution of the composition of the cryolava during the lifetime of the eruptions. Dunes seem to cover part of this flow on its eastern end. We analyze the different terrains using the Spectral Mixing Analysis (SMA) approach of the Multiple-Endmember Linear Unmixing Model (MELSUM, Combe et al., 2008). The study area can be fully modeled by using only two types of terrains. Then, the VIMS spectra are compared with laboratory spectra of known materials in the relevant atmospheric windows (from 1 to 2.78 μm). We considered simple molecules that could be produced during cryovolcanic events, including H₂O, CO₂ (using two different grain sizes), CH₄ and NH₃. We find that the mean spectrum of the cryoflow-like feature is not consistent with pure water ice. It can be best fitted by linear combinations of spectra of the candidate materials, showing that its composition is compatible with a mixture of H₂O, CH₄ and CO₂.

© 2009 Elsevier Ltd. All rights reserved.

1. Introduction

The joint NASA–ESA–ASI Cassini–Huygens mission reached the Saturnian system on July 1st 2004. One of the primary targets of the mission, Saturn's giant moon Titan, is veiled by a dense and hazy atmosphere. Since October 2004, Titan's surface has been imaged by the Cassini radar in Synthetic Aperture Radar (SAR) mode (Elachi et al., 2004), the Cassini Imaging Science Subsystem (ISS) camera (Porco et al., 2005) and the Visual and Infrared Mapping Spectrometer (VIMS, Brown et al., 2004). Numerous geological features have been discovered during the Cassini

nominal mission: dome-like volcanic edifices, flows, and sinuous channels (Elachi et al., 2005), impact craters, networks of fluvial channels and longitudinal dunes (Elachi et al., 2006), resurfacing by cryovolcanism, fluvial erosion, aeolian erosion, and likely atmospheric deposition of materials (Stofan et al., 2006). A detailed review of previous observations is available in Radebaugh et al. (2007). The wealth of geological features makes Titan an Earth-like system with similar processes acting on different materials.

As we report in this paper the joint analysis of VIMS and radar SAR images, we will only describe here these two instruments. The radar experiment can operate as Ku-band SAR at a wavelength (2.7 cm) where Titan's atmosphere is completely transparent. Radar can image Titan's surface with a spatial resolution of approximately 300 m/pixel (Elachi et al., 2005). The radar (in SAR mode) is mainly sensitive to surface roughness, subsurface

* Corresponding author at: Université de Nantes–UFR Sciences et Techniques, LPGNantes UMR 6112 CNRS, 2 rue de la Houssinière, BP 92208, 44322 Nantes, France. Tel.: +33 2 51 12 54 74; fax: +33 2 51 12 52 68.

E-mail address: lucille.le-corre@univ-nantes.fr (L. Le Corre).

structure, dielectric constant variations and topography. It can also probe subsurface materials within 1 m to several meters of the surface assuming a water ice bedrock (Paillou et al., 2006, 2008). VIMS can probe Titan's surface through its dense atmosphere in seven narrow infrared spectral windows (0.93, 1.08, 1.27, 1.59, 2.03, 2.7 and 5 μm), where atmospheric methane absorptions are the weakest. VIMS infrared images are sensitive to composition and grain size, and only probe the first tens of microns of the surface. It can observe Titan from global scale at low to medium resolution (400–25 km/pixel), but it is also able to acquire few spectro-images with a very high spatial resolution when observing at closest approach (up to 500 m/pixel, e.g., Barnes et al., 2008 and this work).

Sotin et al. (2005) described the observations acquired by VIMS of a possible volcanic edifice during the first close flyby of Titan (designated as TA). Later in the mission, larger structures bright at 5 μm in VIMS images were also interpreted as young cryovolcanic regions (Barnes et al., 2005, 2006; McCord et al., 2006). Cryovolcanism (volcanism involving an icy, aqueous or partly crystallized material) is thought to be common on giant planets' icy satellites (Kargel et al., 1991). It can play a major role in their resurfacing, in addition to tectonic processes (Johnson, 2005). On Titan, cryovolcanism may have a significant impact for the replenishment of methane in the atmosphere (Lorenz, 1996; Sotin et al., 2005; Tobie et al., 2006). The detection of ^{40}Ar in the atmosphere and the isotopic ratios $^{13}\text{C}/^{12}\text{C}$ and $^{15}\text{N}/^{14}\text{N}$ strongly suggest exchange processes between the interior and the atmosphere (Tobie et al., 2006), which may include episodes of cryovolcanism.

The Synthetic Aperture Radar has also observed possible cryovolcanic features with associated flows and several calderas during TA, T3, and T8 flybys (Lopes et al., 2007). Few areas have been covered by both VIMS and radar at similar high spatial resolutions, allowing joint studies (e.g., Soderblom et al., 2007a; Barnes et al., 2007; Le Mouélic et al., 2008). Since these instruments are complementary, simultaneous analysis of their datasets can provide key constraints on both the morphology and the composition of surface features.

We focus here on a specific region where a diffuse cryolava flow and its caldera-like feature have been reported in the T3 (February 15, 2005) SAR dataset by Lopes et al. (2007). A fast scanning mode (in the lateral direction, perpendicular to the Cassini groundtrack) was used by VIMS during the T20 closest approach (October 25, 2006) in order to cover a large area with a resolution as high as 500 m/pixel. The T20 VIMS images overlap the T3 flyby SAR swath, allowing the direct comparison between infrared and microwave measurements. Moreover, for the cryo-flow-like feature described in this study, both instruments have similar spatial resolutions, with 760 m/pixel for the VIMS image and about 300 m/pixel for the radar image.

2. Description of VIMS T20 observation

The nominal mode for VIMS operation is to acquire 64×64 pixels cubes using two scanning mirrors with 352 spectroscopic channels covering the spectrum from 0.35 to 5.2 μm (Brown et al., 2004). Because VIMS was not initially designed to image the surface of Titan, most of the planned observations of Titan's surface during the nominal mission are in a ride-along mode with the ISS camera. These observations are usually taken at a few tens of thousands of kilometers from Titan. With a field of view of 0.5 mrd/pixel, the resolution of these observations is often larger than 20 km/pixel.

The best resolutions obtained before T20 were during the first flyby (TA, 26 October 2004) with the imaging of a possible

cryovolcano (Sotin et al., 2005) at 1.7 km/pixel and during the T4 flyby (31 March 2005) with a resolution of 1.4 km/pixel. Since VIMS has shown its capability in mapping Titan's surface during the first flybys, it was decided to use a few closest approach opportunities to observe with VIMS. This new observing strategy has been tested during T20 (25 October 2006), when VIMS was operating for the first time during closest approach at 1030 km from Titan's surface. VIMS detectors took repeated single-line cubes, moving the mirror only in the sample dimension. We therefore relied on the spacecraft motion relative to the moon's surface to build up the second spatial dimension. It corresponds to a fast scanning mode similar to a pushbroom technique. The time exposure was set at its minimum value (13 ms/pixel), and the swath width was varied, ranging from 10 to 24 pixels, in order to obtain a continuous surface coverage over a total length of 1824 pixels (Fig. 1a). This new line mode provides a greater surface coverage and higher spatial resolution than the nominal mode, reaching a spatial resolution of 500 m/pixel at closest approach for this observation.

The subset of the T20 VIMS image that is analyzed in the present study extends from 65.9 to 85.5°W in longitude and from 17 to 24.5°N in latitude (Fig. 1b). It crosses a boundary zone between dark and bright terrains in the equatorial zone. The phase angle varies between 46.1° and 64.9° during the acquisition and the incidence angle ranges from 46.5° to 65.7°. The Sun light comes from the south-east with a sub-solar point located at 14.99°S, 51.50°W (Fig. 1a). For the T20 VIMS image presented in Fig. 1b, the spatial resolution ranges from 665 m/pixel at the lower right to 1.115 km/pixel at the upper left. The data radiometric calibration was optimized using a modified dark frame correction to remove a spurious line-by-line effect. Data have been divided by the cosine of the incidence angle to normalize the lighting geometry to an illumination normal to the surface of the ellipsoid. The southern part of the T20 line mode, which contains numerous dune fields was studied by Barnes et al. (2008).

3. Analysis of VIMS images

3.1. Spatial analysis and correlation with SAR imagery

Noise filtering is applied by performing a Minimum Noise Fraction (MNF). The MNF (Green et al., 1988; Boardman and Kruse, 1994) decorrelates spatially coherent and non-coherent portions of the data, assuming noise is mostly confined in the non-coherent part and rescales the noise by its standard deviation so that its power spectral density has equal power in any band, at any center frequency (noise whitening). A subset of the most coherent MNF bands contains the signal which is the least contaminated by white noise. Finally, an inverse MNF transform reconstitutes data into the space of radiance factor (I/F) and wavelengths. As a result, filtered spectra are smoother, and spectral features are more likely associated to real detection. The results of this MNF treatment have been used primarily to improve the quality of the images in order to clearly identify the boundaries between the different spectral units (Le Mouélic et al., 2007). Maps of spectral criteria have then been computed using bands ratios to minimize albedo and illumination conditions effects. Finally, images were georeferenced using a cylindrical projection (Fig. 1b).

The T20 image is laid over the T3 radar swath (Fig. 1b), which has a spatial resolution ranging from 300 to 1.5 km/pixel (Stofan et al., 2006). Elachi et al. (2006) and Stofan et al. (2006) have described a double ring impact basin (Menvra) and a complex drainage channels pattern (Elivagar Flumina), which appear readily in the left part of Fig. 1b. The T3 radar image also contains a quasi-circular feature with bright rims (feature "A" in Fig. 1b and

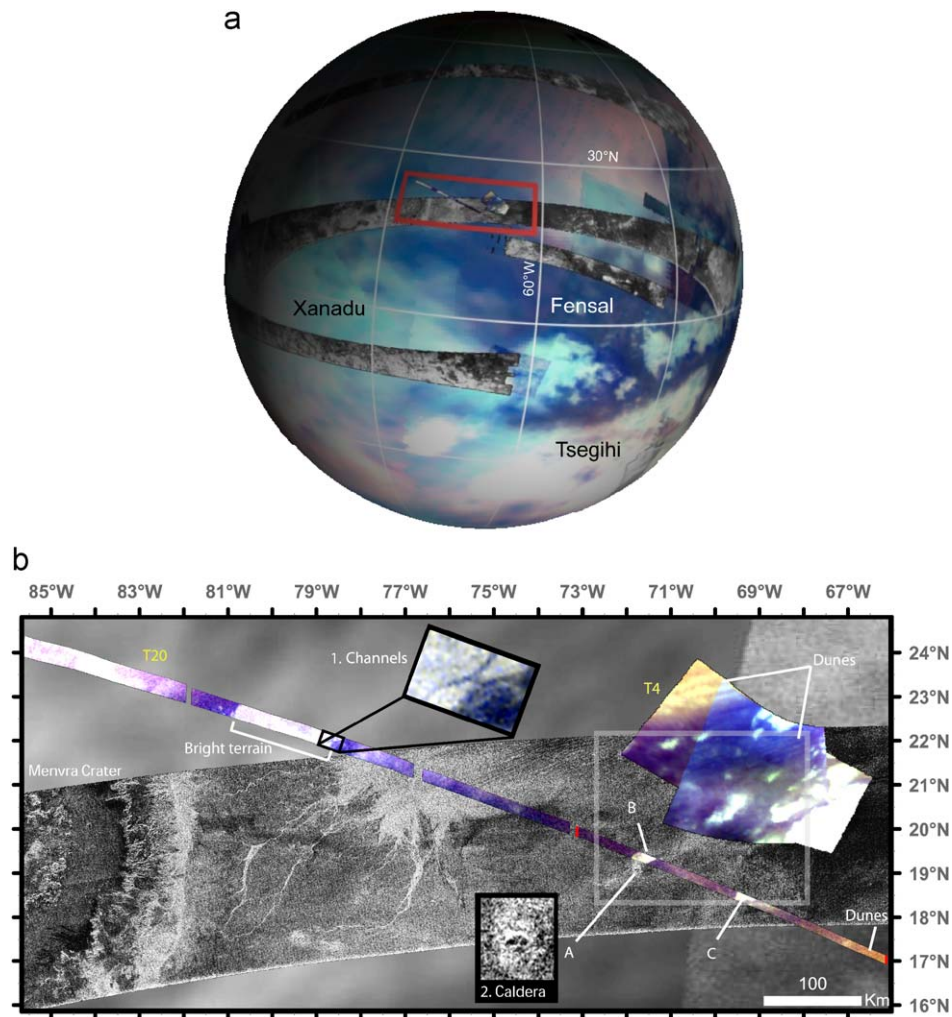


Fig. 1. (a) Orthographic map of Titan centered at 10°N and 70°W , with the illumination conditions during the closest approach of T20 flyby. The VIMS T20 narrow strip is located in the red rectangle. A mosaic of VIMS T8, T9, T13 flybys images is used as background (coded with red as $5\ \mu\text{m}$, green as $2\ \mu\text{m}$, blue as $1.27\ \mu\text{m}$), overlapped by radar SAR images from TA to T19 flybys. (b) VIMS T20 data and VIMS T4 image overlaid on the SAR T3 swath with an ISS background in simple cylindrical geographic projection. The VIMS IR image is a RGB color composite of band ratios with a linear stretch ($R = 1.59/1.27\ \mu\text{m}$, $G = 2.03/1.27\ \mu\text{m}$, $B = 1.27/1.08\ \mu\text{m}$). This color composite emphasizes spectral differences. Channels are seen in the T20 infrared image (zoom no. 1), suggesting that fluvial erosion processes occur on IR-bright material, identified as elevated terrains relative to IR dark terrains. A bright feature (B) is visible on the T3 radar swath, and is also present in the VIMS T20 image. A circular feature (A) located at 20°N 70°W (close up view in the zoom no. 2) seems to be the source of the flow (B) (Lopes et al., 2007). C is another bright feature. The T4 VIMS image clearly shows dunes (Barnes et al., 2008) in the dark regions and distinct bright areas.

the zoom no. 2 showing the caldera), about 8 km in diameter. The inner part of this circular feature is darker than the surroundings in the radar image. This could indicate either a change in surface roughness (smooth at centimeters scale relative to the surroundings) or in composition (with a different dielectric constant of the subsurface). A higher backscattering unit with lobate boundaries (brighter in the radar image) seems to flow out of this feature (Stofan et al., 2006; Lopes et al., 2007). It can be easily seen in the upper image of the Fig. 2, with only the SAR data.

The high-resolution VIMS image has been displayed according to a red–green–blue (RGB) color composite of band ratios ($1.59/1.27$, $2.03/1.27$ and $1.27/1.08\ \mu\text{m}$ ratios, respectively—see Fig. 1b). The different surface spectral units are better distinguished with this color composite (Le Mouélic et al., 2008). The strip starts in the northwest with an infrared (IR) bright area, which is possibly related to Menvra crater seen in the SAR swath. Going in the southeastward direction on the VIMS strip image, a second bright terrain is found. On this IR-bright region, dark lineaments and sinuous patterns appear when the contrast of the image is

enhanced (zoom no. 1 in Fig. 1b captioned as channels). These lineaments are probably related to the large channels network systems at the edges of a very bright feature seen in the underlying radar swath. These images do not allow the clear identification of the complete channels network, but considering the limits in spatial resolution, it seems plausible that we are seeing the main tributaries of a more complex drainage system, such as the ones studied with VIMS by Barnes et al. (2007) and Jaumann et al. (2008), or the ones seen by the Huygens probe (Soderblom et al., 2007b). Further away, the VIMS T20 strip crosses a radar dark region (which has a decreasing reflectance toward the south-east) until a radar bright cryoflow feature is reached. The VIMS IR-bright flow (B) has very sharp boundaries, which are found exactly at the same location than the cryoflow seen in the SAR image (Fig. 2). The IR-bright region B has also a very sharp contrast with the IR dark brown unit. Its width is 12 km. Finally, the strip ends on dunes covering dark ground and bright substrate (Barnes et al., 2008). Dark terrains present two kinds of spectral characteristics, with either brownish or bluish

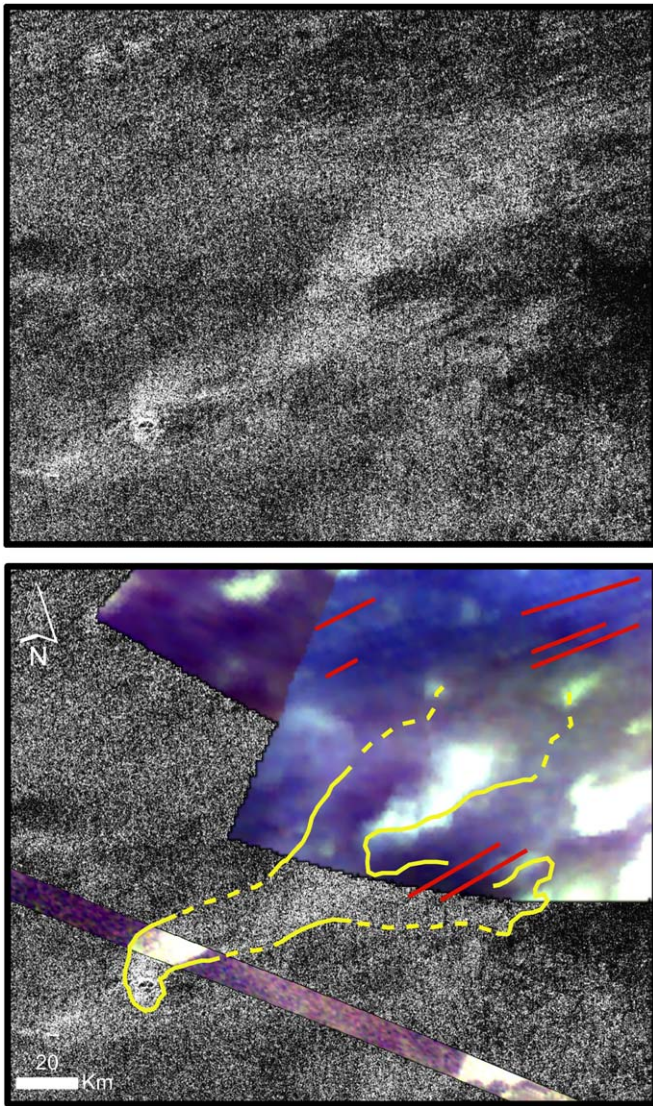


Fig. 2. Close-up view of the caldera and its flow (see the white rectangle in the lower image of Fig. 1b). Top: subset of T3 radar image. Bottom: VIMS T20 and T4 images over the SAR background. The most recognizable dark dunes are underlined with red segments.

tones in our composite images. The dune fields seem to start at the transition between these bluish and brownish tones, at the southeastern end of the strip shown in Fig. 1b. Soderblom et al. (2007a) have been the first to describe that the dunes seen in radar images match the brown and the dark blue IR units at the Huygens landing site. To summarize, by using spectral criteria on the VIMS images and by comparing with SAR image, a good correlation can be found in both datasets between an IR-bright terrain and a cryovolcanic-like radar feature.

3.2. Statistical analysis: search for a specific unit in the cryoflow-like feature with the MELSUM model

The Multiple-Endmember Linear Spectral Unmixing Model (MELSUM) described in Combe et al. (2008) is a Spectral Mixing Analysis (SMA) that uses selected endmember spectra or library spectra to retrieve the distribution of components in an hyperspectral image. This model was first developed to analyze OMEGA Martian data and then applied to Titan VIMS data

(McCord et al., 2008). The model is applied here on the calibrated T20 image by selecting 59 channels in atmospheric windows, from 1 to 2.78 μm . In addition to three artificial constant endmembers, we used as inputs two endmembers in order to run MELSUM on our T20 subset: an average of pixels in dark terrains and another one on bright terrains (see location in Fig. 1b and green and red spectra in Fig. 3). We found that the RMS image of the residuals between the model and the data does not show any spatial coherence, which indicates that, at first order, only two different types of terrains are sufficient to account for the information contained in the infrared image (Fig. 4). This suggests that the cryoflow area is very similar to the bright terrain and the regions observed here by VIMS are, to first order, homogeneous.

Fig. 3 shows a comparison between mean spectra of dark and bright terrains and the cryoflow at T20 (location in Fig. 1) with mean spectra of possible cryovolcanic provinces such as Hotei Regio (Nelson et al., 2009) and Tui Regio (Barnes et al., 2006). These cryovolcanic regions have spectra that are quite different from those of T20, with high signal in all atmospheric windows.

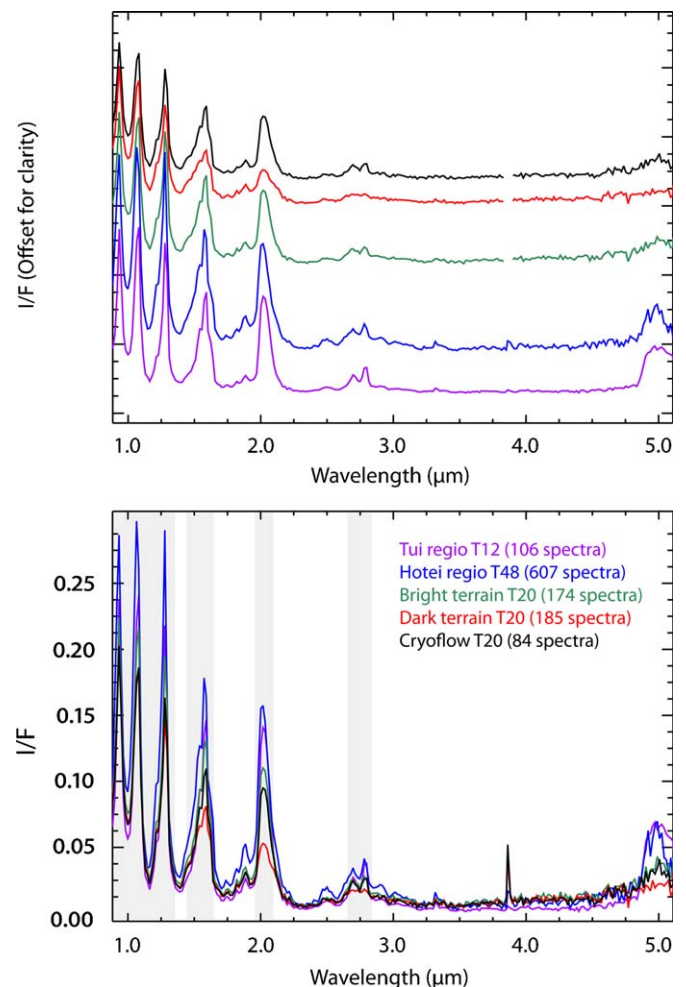


Fig. 3. Comparison between mean spectra of bright and dark areas imaged during T20 flyby with mean spectra of proposed cryovolcanic areas: Tui Regio (Barnes et al., 2006) and Hotei Regio (Nelson et al., 2009). Spectra have been divided by the cosine of the incidence angle to normalize the viewing geometry. With high signal in all atmospheric windows, Tui Regio and Hotei Regio mean spectra are quite different from T20 spectra. The T20 dark terrains (corresponding to dune fields) have the lowest reflectance level at all wavelengths relative to other Titan's units (Barnes et al., 2008). The 59 spectral channels used in the MELSUM model are highlighted in grey color.

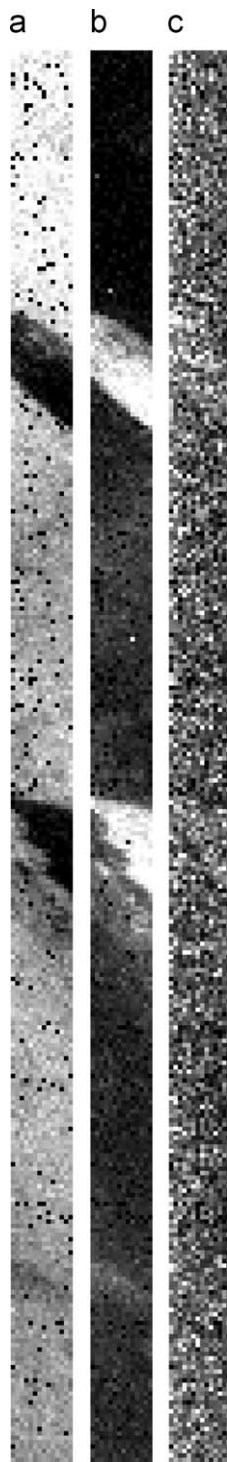


Fig. 4. Images of the results of the MELSUM model applied on the cryoflow region using as input an endmember in the bright terrain and a second on the dark terrain (see its location in Fig. 1b with two red lines indicating the start and the end of this part of the T20 strip image). (a) Mixing coefficient for the dark terrain endmember. (b) Mixing coefficient for the bright terrain endmember. (c) RMS. No spatial feature is seen in the RMS image, which shows that the two endmembers selected are sufficient to account for the observed variability in this T20 image.

3.3. Spectral analysis and comparison with modeled spectra of ices

3.3.1. Comparison with spectra of pure ices

Fig. 5 shows a set of averaged spectra representative of the main units (same selected regions than in Fig. 3, see Fig. 1b for location). Due to the very short integration time, spectra in this

particular sequence contain high instrumental noise, especially affecting wavelengths greater than $3\ \mu\text{m}$ where the signal is very low (few DN). To improve the signal-to-noise ratio, we average spectra over selected regions (Fig. 1b): 174 spectra over a bright terrain, 84 spectra over the cryoflow-like feature (B), and 185 spectra over the dark terrain. The spectra do not cross each other in the seven methane windows, suggesting that the bright unit, the cryoflow and the dark background do not differ markedly in their superficial composition. However, the relative brightness varies in each of the seven infrared windows: the dark material displays a steeper negative spectral slope between 1.59 and $2.03\ \mu\text{m}$ windows and the bright terrains have a positive spectral slope between 2.7 and $2.8\ \mu\text{m}$ compared to a relatively similar brightness at 2.7 and $2.8\ \mu\text{m}$ for the dark terrains. The quantification of spectral differences using the Spectral Angle Mapper (SAM) procedure of ENVI (Kruse, 1993) in 59 selected spectral channels in the methane windows, demonstrates that the cryoflow mean spectrum is closer to the bright unit mean spectrum than the dark unit mean spectrum (with an angular distance of 0.032 and 0.148 rad, respectively). Therefore, the dark terrains may contain a chemical component that darkens their spectra in the $2.03\ \mu\text{m}$ spectral window and in the 2.69 – $2.78\ \mu\text{m}$ range.

The comparison between VIMS spectra and spectra of plausible ice candidates in the most discriminative atmospheric spectral windows (at 1.59 , 2.03 and $2.7\ \mu\text{m}$) brings some clues about the chemical composition. We calculated several spectra of pure candidate ices in order to attempt to match the general shape of the VIMS spectra. These ice components have been suggested in previous spectral studies from ground-based telescopes or Cassini instruments. Pure CO_2 ice or CO_2 ice mixed with H_2O ice have been put forward by interpreting the positive spectral slope across the double atmospheric window at 2.73 and $2.77\ \mu\text{m}$ (Coustenis et al., 2006; McCord et al., 2008), the high reflectance in the $5\ \mu\text{m}$ spectral window (Barnes et al., 2005; McCord et al., 2008), an absorption band at $4.92\ \mu\text{m}$ (McCord et al., 2008) and small absorption features at 1.55 and $1.62\ \mu\text{m}$ (Rodriguez et al., 2006). H_2O ice (or relative enrichment in H_2O ice) was also suggested when arguing for the relative reflectance at 1.3 , 1.6 and $2.0\ \mu\text{m}$ (Coustenis et al., 1995; Griffith et al., 2003; Rodriguez et al., 2006; Soderblom et al., 2007a; McCord et al., 2006, 2008; Buratti et al., 2007) and was detected with DISR instrument (Tomasko et al., 2005). NH_3 can be also responsible for the relative reflectance at 1.3 , 1.6 and $2.0\ \mu\text{m}$ (Griffith et al., 2003; Soderblom et al., 2007a; Fortes et al., 2007; Nelson et al., 2009).

Fig. 5 (top left) shows reflectance spectra computed for candidate compounds using optical constants of pure ices calculated with the method described in Lucey (1998). It relies on approximations of the radiative transfer theory (Chandrasekhar, 1960) by Hapke (1993). This method was originally developed for computing optical constants of minerals (olivine and pyroxene) with the assumptions that the internal scattering coefficient is set to zero. This model does not take into account the property of multiple scattering for ices, which could modify the spectral contrast. The multiple scattering decreases globally the reflectance of a surface. We can compensate this drawback by using larger grain size in order to reduce the contrast in the modeled spectra. A larger grain size used in our model set of parameters permits to increase the effect of absorptions in the spectra, which is nearly equivalent at first order to a multiple scattering effect by reducing the overall contrast. We focus here on the shape of the spectra rather than trying to retrieve the grain size of the materials. Optical constants from Grundy et al. (2002) for CH_4 at $40\ \text{K}$, from Quirico and Schmitt (1997) for CO_2 at $30\ \text{K}$, and from Schmitt et al. (1998) for NH_3 at $40\ \text{K}$ and from Grundy and Schmitt (1998) and Schmitt et al. (1998) for H_2O at 40 – $60\ \text{K}$

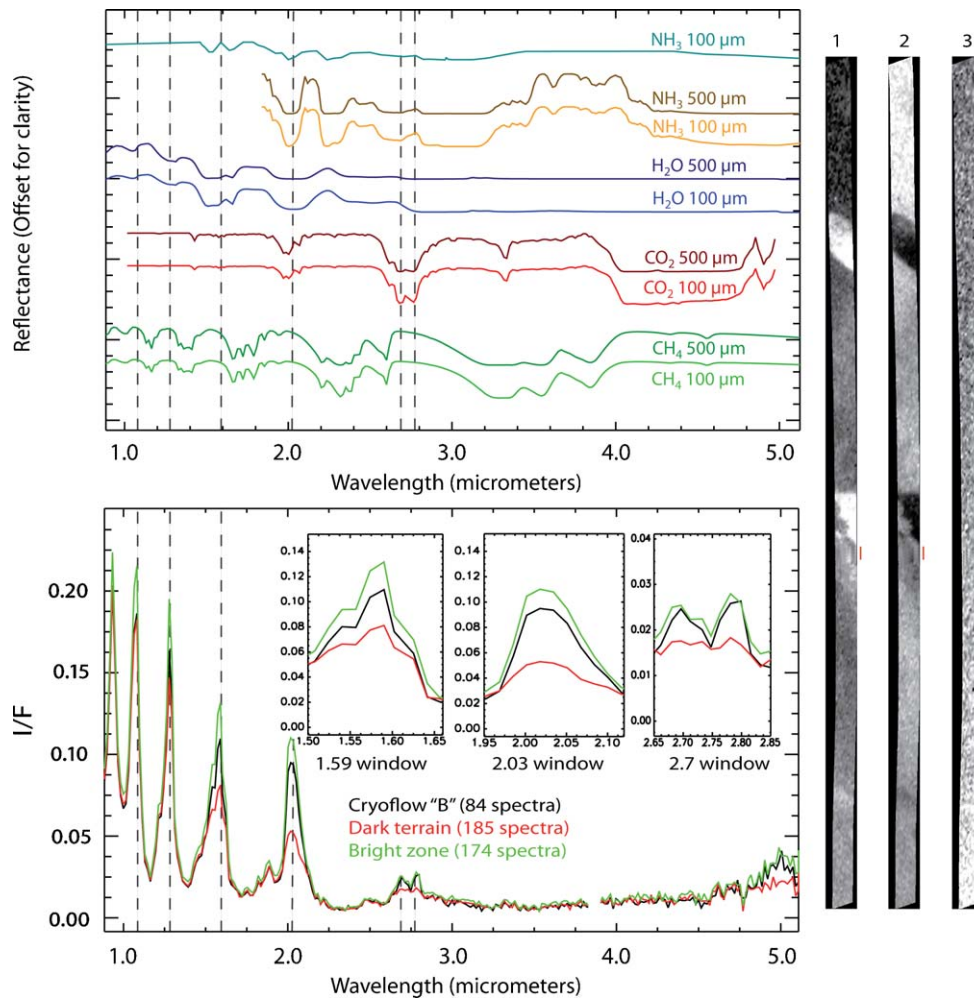


Fig. 5. Right: subset of T20 inbound swath in simple cylindrical projection, (1): 2.03/1.27 μm ratio, (2): 2.69/2.78 μm ratio, (3): 1.90 μm channel. The lack of coherent feature at 1.9 μm demonstrates that the observed features are not related to tropospheric clouds. The two bright features in strip (1) correspond to features (B) and (C) in Fig. 1b. The red segments indicate geometrically interpolated data. Top left: infrared spectra of four candidate molecules for Titan solid surface, modeled for a grain size of 100 and 500 μm , resampled at VIMS resolution. In order to complete the ammonia spectrum for short wavelengths, we computed a second spectrum with refractive index at $\sim 80\text{K}$ obtained using the dataset described in Martonchik et al. (1984). The grey dashed lines indicate the central wavelengths of the spectral windows relevant to the discussion. Bottom left: averaged spectra of flow "B", bright terrain and dark terrain (see Fig. 1b to locate each unit). No significant spectral variations are observed. However, there is a difference in slope between the 2.69 and 2.78 μm windows between bright and dark terrains. None of the pure ice candidates gives a reasonable fit to the observed Titan spectra.

(depending on the wavelength range), were used to calculate single scattering albedo for a given grain size. The single scattering albedo was converted into reflectance spectra assuming a viewing geometry similar to the T20 data conditions (with a mean phase angle of 55° calculated using ancillary data over the strip) and an isotropic single scattering phase function. The synthetic spectra can slightly differ depending on the theoretical model used to retrieve the reflectance and the chosen optical constants, which can be substantially modified according to the film thickness or temperature range used for the measurements (Schmitt et al., 1998). Even if we do not take into account the multiple scattering in our model, the spectra are consistent with spectra found in the literature (Langevin et al., 2005; Rodriguez et al., 2006).

Spectra of ices with grain sizes of 100 and 500 μm are displayed in Fig. 5. A NH₃ spectrum derived from Martonchik et al. (1984) has been added to cover the 1.0 to 1.8 μm wavelength range. All spectra were resampled at VIMS spectral resolution. Titan surface's temperature is $\sim 94\text{K}$ (Fulchignoni et al., 2005) and temperatures used in laboratory data to derive the optical constant of pure ice spectra are 40, 30, and 60K. In the spectral

range of our study, these experimental measurements are the closest to Titan's surface temperature that are currently available in the published literature.

3.3.2. Discussion using image ratios

It is possible to rule out atmospheric effects such as the presence of tropospheric clouds (above $\sim 30\text{km}$) by scanning the wings of the 2 μm methane window (Griffith et al., 2006). The lack of coherent feature at 1.9 μm (strip number 3 in Fig. 5) demonstrates that the observed features are not related to tropospheric clouds and are therefore directly linked to the surface.

Several conclusions can be drawn by comparing data from 2.69 and 2.78 μm windows with the modeled spectra of pure candidates ices presented in the previous section. Dark terrains display almost equal reflectance levels at these wavelengths, whereas bright regions display rather a positive slope between these two wavelengths. It must be noted that the absorption feature seen at 2.75 μm is probably related to the atmosphere (may be due to absorption by aerosols or gas other than methane),

as the same feature can be detected in clouds' spectra. Pure water ice has a negative slope in this spectral region. Titan spectra are therefore not consistent with pure water ice spectra as demonstrated by Rodriguez et al. (2006) and McCord et al. (2006). This is also confirmed on false colors images. Indeed, the image ratio of 2.69/2.78 in Fig. 5 (right) displays the darkest tones for the zones B and C. Pure water ice exposures would show up as bright terrains due to the negative spectral slope between these two spectral channels. The same argument cannot be definitive for solid methane, which has a 2.69/2.78 ratio around 1. CO₂ can account for the observed positive slope considering 100 μm grain size. Previously, McCord et al. (2008) suggested CO₂ ice with 10 μm grain size to fit the contrast between the 2.69 and 2.78 μm windows. For a grain size equal to 500 μm, the signal is very low and the ratio is close to 1. Ammonia has a positive spectral slope in this wavelength range, which makes it also a good candidate if this criterion is used alone.

Other spectral properties may be evaluated to provide additional constraints on the surface composition. The 1.59/1.27, 2.03/1.27, and 1.27/1.08 μm ratios are displayed in red, green and blue, respectively, in Figs. 1 and 3. Water ice absorbs at 1.59 and 2.03 μm, but not at 1.27 μm, which leads to link the blue color to a possible enrichment in water ice, as argued by Rodriguez et al. (2006). Therefore, the material building up the cryoflow is not consistent with pure water ice as also discussed previously. Since ammonia absorbs at 2.03 μm, its presence should give a violet color, which is not seen in the bright flow, ruling out ammonia as being present as pure ice in the flow feature.

3.3.3. Comparison with modeled spectra of mixtures of ices in the Titan viewing conditions

As none of the pure ices gives a reasonable fit to the observed spectra, we then considered mixtures of ices. Since the absorption by the atmospheric methane gas is the prevailing effect on the VIMS spectra, our synthetic mixture spectra have also been multiplied by a simulated transmission of a quantity of methane gas corresponding to the VIMS viewing conditions of the cryoflow during T20 flyby (with an incidence angle of 52.13° and an emergence angle of 1.82°), using the total opacity of methane gas in Titan's atmosphere (P. Rannou, private communication).

Two other atmospheric components can contribute to the shape of the spectra seen by VIMS: N₂ and CO. A N₂ wide absorption is present as the consequence of the collision-induced phenomenon in the ~3.84–4.76 μm range (Shaw, 1970), within the methane and CO absorption ranges that already absorb the reflectance signal. A second absorption occurs between 2.05 and 2.45 μm, on the right wing of the 2.03 μm window, and is absorbing the signal more than the methane (Negrão, 2007, see Fig. 5.9). CO affects the 5 μm atmospheric window of the VIMS spectra, especially the wing of the window by absorbing in the range ~4.48–4.88 μm (Shaw, 1970).

An additive component must be added in order to take into account the scattering by atmospheric particles. The empirical approach suggested by Rodriguez et al. (2006) cannot be applied here because there is no signal in the 5 μm window due to the short integration time (~0.5 DN). An alternative model, also presented in Rodriguez et al. (2006), computes the value of the backscattering coefficient in a given spectral channel taking into account the geometry of observation. In this calculation, the layer of aerosols is considered as a homogeneous layer of 0.15 μm radius particles with a 100 cm⁻³ density and a thickness of 200 km. The mean curve of the additive component on the cryoflow feature is computed and then added for each 256 wavelengths of the synthetic spectra. This must be done before multiplying the modeled spectra by the transmission function of atmospheric

methane. Finally, a normalization factor is applied to the modeled spectra to scale them to the VIMS reflectance level.

Synthetic spectra of ices mixtures are computed with grain sizes of 500 μm for H₂O, CH₄ and NH₃ and two different grain sizes of 500 and 100 μm for CO₂. As discussed previously, this kind of model overestimates grain sizes. The calculation gives several mixtures of ices attributing to each ice a different proportion coefficient from 0 to 0.75 with a step value of 0.25 to limit the number of synthetic spectra. A systematic comparison between modeled spectra and the VIMS mean spectrum of the cryoflow is performed in order to select the most relevant synthetic spectra of mixture of ices. The SAM was used to select the spectra that best fit the mean spectrum of the cryoflow. Considering that for ammonia we only have access to optical constants between 1.9 and 5 μm, we performed the SAM method for mixtures without ammonia between 1 and 2.82 μm (51 spectral channels), and for mixtures containing ammonia and without ammonia: between 1.9 and 2.82 μm (19 spectral channels). We selected spectral channels within the methane windows and the 3–5.11 μm range was not considered since the signal-to-noise ratio is too low. The first analysis including 51 bands gave angle values from 0.52 to 0.74 rad. The reflectance at short wavelengths (in the 1.08 and 1.27 μm windows) has a high value relative to VIMS T20 spectra for all selected mixtures of ices. That could be due to absorption by another dark component on the surface of Titan that we did not consider. Alternatively, in our synthetic spectra, there may be an overestimate of the transmission or of the reflectance of ices. There may exist an additional component that absorbs in the left wings of the 1.59 μm window, as we do not reproduce well its shape. For the 2.03 μm window, the mixtures computed here have a general good agreement, except that the right part of this window is affected in VIMS data by the N₂ absorption, which is not considered in our model. The shape of the 2.69 and 2.78 μm windows are well fitted by the mixtures proposed in Fig. 6a. Then, we considered the SAM analysis with 19 channels to see whether or not ice mixtures containing NH₃ could fit better this part of the 1.9–2.82 μm range of the cryoflow mean spectrum. This analysis calculated angles from 0.39 to 1.08 rad. In this case, the lower angles are found (from 0.39 to 0.53 rad) for mixtures containing CH₄ plus CO₂ or H₂O, CH₄, and CO₂. The best mixture containing ammonia has an angle of 0.51 rad, and this value increases until 1.08 when the proportion of ammonia increases. Therefore, we can rule out ammonia mixtures as a principal component in our selection of spectra. Taking into account the 51 bands, the first 9 spectra were selected (Fig. 6a and b) to further analysis (with an angle ranging from 0.519 to 0.534 rad). The final selection is then performed by using the RMS calculation of the residuals found between each synthetic spectrum and the mean cryoflow spectrum with the same selection of 51 bands (Fig. 6c). The RMS ranges from 0.0242 to 0.0247 for the selection of the Fig. 6a. Among this selection, we ruled out a spectrum which presents a negative slope in the 2.69–2.78 μm range, since the cryoflow feature has a positive slope in this wavelength range. The two most relevant mixtures are either (25% H₂O; 25% CO₂ (500 μm); 50% CH₄) or (25% H₂O; 50% CO₂ (100 μm); 25% CH₄) (Fig. 6d).

The conclusion of this first-order analysis dealing with four simple molecules that are thought to be present on Titan is that mixtures containing H₂O, CH₄, and CO₂ are a possibility to account for the shape of the VIMS spectra of the cryoflow feature.

4. Implications for Titan's geology

The bright lobate feature seen in Fig. 1 has been interpreted as a cryovolcanic flow with a caldera-like feature located to the East of T20 image (Lopes et al., 2007). According to the radar data, it

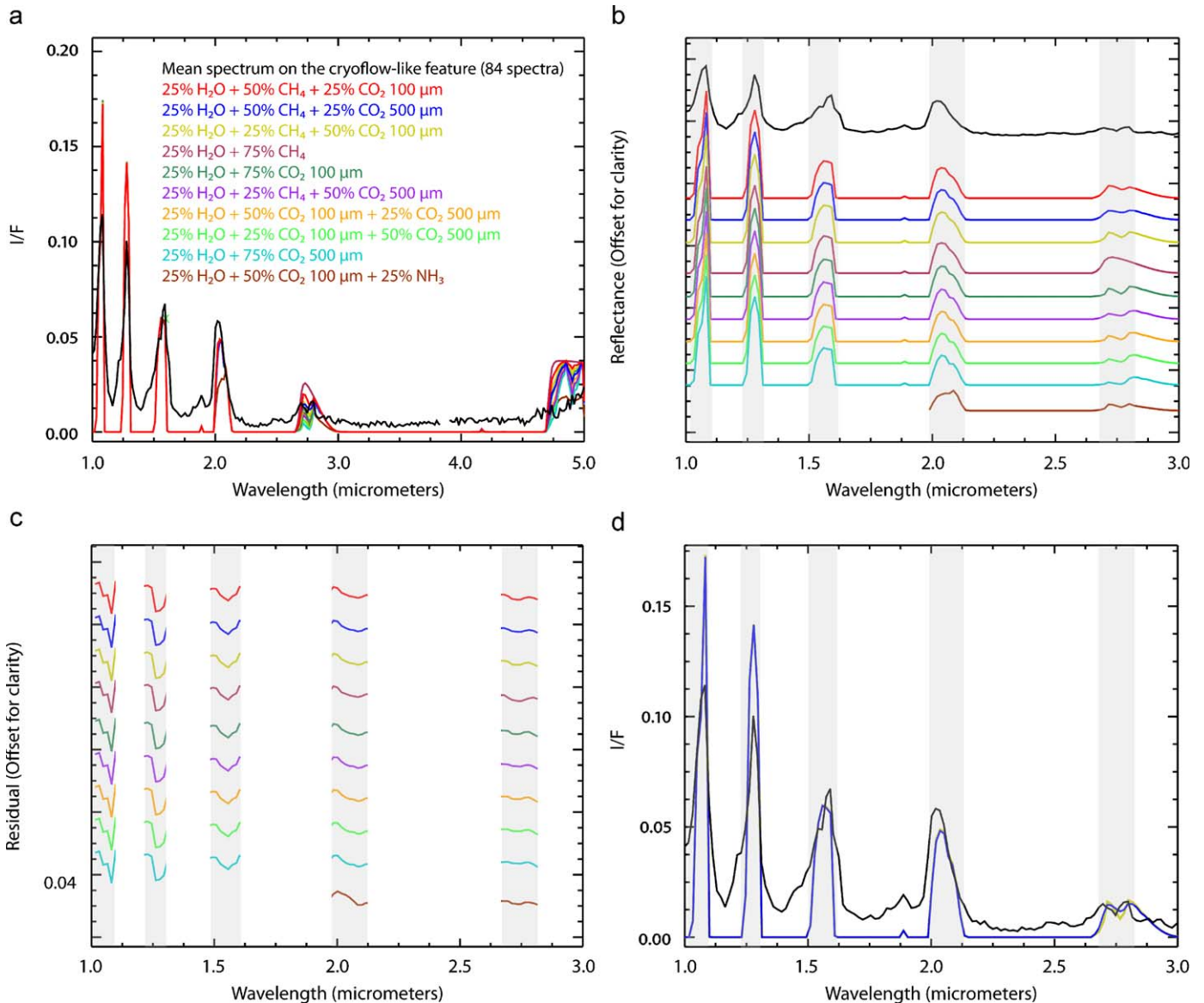


Fig. 6. Comparison between the mean spectrum of the T20 cryoflow with modeled spectra of several ices mixtures with addition of the additive backscattering coefficient derived using Rodriguez et al. (2006) model, convolved by the atmospheric methane transmission in the T20 viewing condition. Spectra have been normalized for comparison. When calculated with a fraction of ammonia, synthetic spectra begin at 2 μm because optical constants are missing in the range 1–2 μm at 40 K. The graphic (a) presents the preliminary selection of mixtures of ices (we added also an example of ice mixture containing ammonia, that does not fit the 2 μm window). The second graphic (b) presents an offset with the same spectra. The grey color indicates the spectral ranges used for the selection. The residuals between the cryoflow mean spectrum and each synthetic spectra (calculated within the atmospheric windows) are shown in (c). The two most relevant spectra are selected in (d). Whereas it does not give a perfect match, the best fit is obtained by the two mixtures: (25% H₂O; 25% CO₂ (500 μm); 50% CH₄) or (25% H₂O; 50% CO₂ (100 μm); 25% CH₄).

seems to have flown over a distance of 160 km, which implies that the corresponding cryolava must have a low viscosity. The flow originating from this caldera is globally oriented in the northeast direction is 12–80 km wide. The whole structure covers an area of about $\sim 5500 \text{ km}^2$. There is a strong correlation in location and brightness between the radar data and the optical image. It could imply either that (i) the surface roughness is high at 2 cm and that surface here is highly reflective in the infrared windows, or (ii) the cryolava has a different chemical composition as the surrounding terrain, or (iii) there is an unaccounted topographic effect. Compared to other areas which are bright in the optical wavelengths and dark in radar (Soderblom et al., 2007a), this correlation might indicate that the flow has not yet been degraded by erosion or weathering processes. Towards the eastern end of the flow, it is covered by longitudinal dunes in the radar dark

region in Fig. 2 and appears dark in the composite image. Thus, the flow is to be considered as relatively old if we look at the part covered up by dunes; but not so old because the proximal area near the putative vent, shows strong VIMS/radar correlation, perhaps implying a more youthful feature.

The present analysis suggests that the flow is composed of a mixture of different ices. In addition, this kind of flow may release methane in the atmosphere if this compound is present at depth (Tobie et al., 2006). Such a structure is compatible with the presence of an upwelling plume that would trigger the destabilization of clathrate hydrates at a few kilometers depth. However, the amount of methane that can be released by this process is several orders of magnitude smaller than the amount existing in the atmosphere, considering the fact that only few small features have been found so far. However, VIMS has imaged only $\sim 2\%$ of

Titan's surface at a resolution low enough to detect such features. But they should have been seen by the radar, unless their degradation hides them from remote sensing observations, making only the most recent ones being observable. It is worth noting that VIMS observed large 5 μm bright structures like Tui or Hotei Regio, which are thought to have a cryovolcanic origin. The cryovolcanic origin of Hotei Regio is also supported by radar SAR observations that show lobate flow features (Wall et al., 2009). The destabilization of methane clathrates and CO_2 ices in the crust below one of the large 5 μm bright structures could provide enough methane to permit the recycling of the atmosphere over Titan's history. It has also been proposed that the lakes may provide enough ethane and methane (Mitri et al., 2007). However, estimates by Lorenz et al. (2008) suggest that the evaporation of these reservoirs is not sufficient to replenish the amount of methane gas in the atmosphere over geologic timescales.

5. Conclusion

The VIMS data acquired during the T20 flyby with a spatial resolution of 500 m/pixel show a bright area with very sharp boundaries that is spatially correlated with a bright feature previously observed by the radar during the T3 flyby, interpreted as cryovolcanic flow originating from a small circular feature seen nearby in SAR data (Lopes et al., 2007). While the exact chemical composition of the corresponding materials cannot be identified using present laboratory information, some constraints can be placed on the material composition. The infrared reflectance of the flow is inconsistent with pure H_2O , CH_4 , CO_2 and NH_3 ices. Even if two different grain size ranges are used, none of the candidates completely fulfils all criteria. It seems that the regions observed in the T20 flyby are covered by a material that makes the spectral signatures of all the terrains quite similar to each other, except for the overall level of the spectra. It might be consistent with the idea of an air fall deposit of aerosols, which make up the bright terrains; whereas the dunes and the IR dark terrains would contain a more evolved form of this air fall deposit (Soderblom et al., 2007a). According to this hypothesis, IR-bright terrain should be transparent to radar, whereas a bright cryoflow (as in our study) would show up rather bright in radar images. As for the modeled spectra of mixtures of ices, we found a better match for mixtures containing H_2O , CO_2 and CH_4 ices. Spectra with two different grain sizes for CO_2 ice are also a way to explain the shape of VIMS spectra (as suggested by McCord et al. 2008). Nonetheless, it is necessary to improve the atmospheric correction (haze scattering, methane absorption) using a more accurate radiative transfer code to interpret the subtle variability in the spectral signatures. Different kinds of hydrocarbons and nitriles are also expected to be present at the surface (Atreya et al., 2006). The recent laboratory measurements of hydrocarbons by Clark et al. (2009) will be very useful to improve the identification of the materials building up the surface of Titan. More VIMS T20-like high-resolution images in the forthcoming flybys merged on the radar background would provide strong constraints for understanding the composition and morphology of geological features, as well as the cryovolcanic processes.

Acknowledgments

The author wish to thank Pascal Rannou for providing the total optical depth of methane in the atmosphere of Titan. The first author would like to thank Nantes Métropole for her Ph.D. grant. Thanks to the VIMS team for getting the data. We also thank T.

McCord and G. Hansen for their constructive comments on a previous version of this paper. A part of this work was carried out at JPL under contract with NASA. Support by the French Space Agency (CNES) is greatly appreciated.

References

- Atreya, S.K., Adams, E.Y., Niemann, H.B., Demick-Montelara, J.E., Owen, T.C., Fulchignoni, M., Ferri, F., Wilson, E.H., 2006. Titan's methane cycle. *Planet. Space Sci.* 54, 1177–1187.
- Barnes, J.W., et al., 2005. A 5-micron-bright spot on Titan: evidence for surface diversity. *Science* 310, 92–95 doi:10.1126/science.1117075.
- Barnes, J.W., et al., 2006. Cassini observations of flow-like features in western Tui Regio, Titan. *Geophys. Res. Lett.* 33, L16204.
- Barnes, J.W., et al., 2007. Near-infrared spectral mapping of Titan's mountains and channels. *J. Geophys. Res.* 112, E11006.
- Barnes, J.W., et al., 2008. Spectroscopy, morphometry, and photogrammetry of Titan's dunefields from Cassini/VIMS. *Icarus* 195, 400–414.
- Boardman, J.W., Kruse, F.A., 1994. Automated spectral analysis: a geological example using AVIRIS data, north Grapevine Mountains, Nevada: in: Proceedings, ERIM Tenth Thematic Conference on Geologic Remote Sensing, Environmental Research Institute of Michigan, Ann Arbor, MI, pp. 1-407–1-418.
- Brown, R.H., Baines, K.H., Bellucci, G., Bibring, J.P., Buratti, B.J., Bussoletti, E., Capaccioni, F., Cerroni, P., Clark, R.N., Coradini, A., Cruikshank, D.P., Drossart, P., Formisano, V., Jaumann, R., Langevin, Y., Matson, D.L., McCord, T.B., Mennella, V., Miller, E., Nelson, R.M., Nicholson, P.D., Sicardy, B., Sotin, C., 2004. The Cassini visual and infrared mapping spectrometer investigation. *Space Sci. Rev.* 115, 111–168.
- Buratti, B.J., Pitman, K.M., Brown, R.H., Barnes, J.W., Baines, K., Clark, R., Jaumann, R., Nicholson, P., Sotin, C., 2007. Exploring Methods to Rule Out Surface Compositional Types on Titan Using Cassini VIMS T20 Data. 38th Lunar and Planetary Science Conference, abstract no. 1165.
- Chandrasekhar, S., 1960. Radiative Transfer. Dover, New York.
- Clark, R.N., Curchin, J.M., Hoefen, T.M., Swayze, G.A., 2009. Reflectance Spectroscopy of Organic Compounds I: Alkanes. *J. Geophys. Res.* 114, E03001, doi:10.1029/2008JE003150.
- Combe, J.-Ph., Le Mouélic, S., Sotin, C., Gendrin, A., Mustard, J.F., Le Deit, L., Launeau, P., Bibring, J.-P., Gondet, B., Langevin, Y., Pinet, P., and the OMEGA Science team, 2008. Analysis of OMEGA/Mars Express data hyperspectral data using a Multiple-Endmember Linear Spectral Unmixing Model (MELSUM): Methodology and first results. *Planetary and Space Science* 56, 951–975, doi:10.1016/j.pss.2007.12.007.
- Coustonis, A., Lellouch, E., Maillard, J.P., McKay, C.P., 1995. Titan's surface: composition and variability from the near-infrared albedo. *Icarus* 118, 87–104.
- Coustonis, A., Negrão, A., Salama, A., Schulz, B., Lellouch, E., Rannou, P., Drossart, P., Encrenaz, T., Schmitt, B., Boudon, V., Nikitin, A., 2006. Titan's 3-micron spectral region from ISO high-resolution spectroscopy. *Icarus* 180, 176–185.
- Elachi, C., et al., 2004. Radar: the Cassini Titan radar mapper. *Space Sci. Rev.* 117, 71–110.
- Elachi, C., Wall, S., Allison, M., Anderson, Y., Boehmer, R., Callahan, P., Encrenaz, P., Flamini, E., Franceschetti, G., Gim, Y., Hamilton, G., Hensley, S., Janssen, M., Johnson, W., Kelleher, K., Kirk, R., Lopes, R., Lorenz, R., Lunine, J., Muhleman, D., Ostro, S., Paganelli, F., Picardi, G., Posa, F., Roth, L., Seu, R., Shaffer, S., Soderblom, L., Stiles, B., Stofan, E., Vetrilla, S., West, R., Wood, C., Wye, L., Zebker, H., 2005. Cassini radar views the surface of Titan. *Science* 308, 970–974.
- Elachi, C., et al., 2006. Titan radar mapper observations from Cassini's T3 fly-by. *Nature*, 441.
- Fortes, A.D., Grindrod, P.M., Trickett, S.K., Vočadlo, L., 2007. Ammonium sulfate on Titan: possible origin and role in cryovolcanism. *Icarus* 188, 139–153.
- Fulchignoni, M., et al., 2005. In situ measurements of the physical characteristics of Titan's environment. *Nature* 438, 785–791.
- Green, A.A., Berman, M., Switzer, P., Craig, M.D., 1988. A transformation for ordering multispectral data in terms of image quality with implications for noise removal. *IEEE Trans. Geosci. Remote Sensing* 26 (1), 65–74.
- Griffith, C.A., Owen, T., Geballe, T.R., Rayner, J., Rannou, P., 2003. Evidence for the exposure of water ice on Titan's surface. *Science* 300, 628–630.
- Griffith, C.A., et al., 2006. Evidence for a polar ethane cloud on Titan. *Science* 313, 1620–1622.
- Grundy, W.M., Schmitt, B., 1998. The temperature-dependent near-infrared absorption spectrum of hexagonal H_2O ice. *J. Geophys. Res.* 103 (25), 809–822.
- Grundy, W., Schmitt, B., Quirico, E., 2002. The temperature dependent spectrum of methane ice I between 0.7 and 5 mm and opportunities for near-infrared remote thermometry. *Icarus* 155, 486–496.
- Hapke, B., 1993. Theory of Reflectance and Emission Spectroscopy. Topics in Remote Sensing. Cambridge University Press, Cambridge, UK.
- Jaumann, R., Brown, R.H., Stephan, K., Soderblom, L.A., Sotin, C., Le Mouélic, S., Barnes, J.W., Clark, R.N., Buratti, B.J., Wagner, R., McCord, T.B., Rodriguez, S., Baines, K.H., Cruikshank, D.P., Nicholson, P.D., Griffith, C.A., 2008. Fluvial erosion and post-erosional processes on Titan. *Icarus* 197, 526–538.
- Johnson, T.V., 2005. Geology of the icy satellites. *Space Sci. Rev.* 116, 401–420.

- Kargel, J.S., Croft, S.K., Lunine, J.I., Lewis, J.S., 1991. Rheological properties of ammonia–water liquids and crystal–liquid slurries—Planetological applications. *Icarus* 89, 93–112.
- Kruse, F.A., 1993. The Spectral Image Processing System (SIPS)—Interactive Visualization and Analysis of Imaging spectrometer data. *Remote Sensing of Environment* 44, 145–163.
- Langevin, Y., Poulet, F., Bibring, J.-P., Schmitt, B., Douté, S., Gondet, B., 2005. Summer evolution of the north polar cap of Mars as observed by OMEGA/Mars express. *Science* 307, 1581–1584.
- Le Mouélic, S., Sotin, C., Rodriguez, S., Tobie, G., Le Corre, L., Brown, R.H., Barnes, J.W., Soderblom, L., Jaumann, R., Baines, K.H., Clark, R., Nicholson, P.D., 2007. Spatial and Spectral Filtering Strategies for Cassini VIMS Surface Images of Titan. 38th LPSC, Houston, abstract# 1574.
- Le Mouélic, S., et al., 2008. Joint analysis of Cassini VIMS and RADAR data: application of the mapping of Sinlap crater on Titan. *J. Geophys. Res.*, 113.
- Lopes, R.M.C., et al., 2007. Cryovolcanic features on Titan's surface as revealed by the Cassini Titan radar mapper. *Icarus* 186, 395–412.
- Lorenz, R.L., 1996. Pillow lava on Titan, expectations and constraints on cryovolcanic processes. *Planet. Space Sci.* 44, 1021–1028.
- Lorenz, R.D., Mitchell, K.L., Kirk, R.L., Hayes, A.G., Aharonson, O., Zebker, H.A., Paillou, Ph., Radebaugh, J., Lunine, J.I., Janssen, M.A., Wall, S.D., Lopes, R.M., Stiles, B., Ostro, S., Mitri, G., Stofan, E.R., 2008. Titan's inventory of organic surface materials. *Geophys. Res. Lett.* 35, 2.
- Lucey, P.G., 1998. Model near-infrared optical constants of olivine and pyroxene as a function of iron content. *J. Geophys. Res.* 103, 1703–1713.
- McCord, T.B., Hansen, G.B., Buratti, B.J., Clark, R.N., Cruikshank, D.P., D'Aversa, E., Griffith, C.A., Baines, E.K.H., Brown, R.H., Dalle Ore, C.M., Filacchione, G., Formisano, V., Hibbitts, C.A., Jaumann, R., Lunine, J.I., Nelson, R.M., Sotin, C., the Cassini VIMS Team, 2006. Composition of Titan's surface from Cassini VIMS. *Planet. Space Sci.* 54, 1524–1539.
- McCord, T.B., Hayne, P., Combe, J.-Ph., Hansen, G.B., Barnes, J.W., Rodriguez, S., Le Mouélic, S., Baines, E.K.H., Buratti, B.J., Sotin, C., Nicholson, Ph., Jaumann, R., Nelson, R., The Cassini Vims Team, 2008. Titan's surface: search for spectral diversity and composition using the Cassini VIMS investigation. *Icarus* 194, 212–242.
- Martonchik, J.V., Orton, G.S., Appleby, J.F., 1984. Optical properties of NH₃ ice from the far infrared to the near ultraviolet. *Appl. Opt.* 23 (4), 541–547.
- Mitri, G., Showman, A.P., Lunine, J.I., Lorenz, R.D., 2007. Hydrocarbon lakes on Titan. *Icarus* 186, 385–394.
- Negrão, A., 2007. The characterisation of Titan's lower atmosphere and surface from near-infrared spectra. Ph.D. Thesis, university of Lisboa.
- Nelson, R.M., Kamp, L.W., Matson, D.L., Irwin, P.G.J., Baines, K.H., Boryta, M.D., Leader, F.E., Jaumann, J., Smythe, W.D., Sotin, C., Clark, R.N., Cruikshank, D.P., Drossart, P., Pearl, J.C., Hapke, B.W., Lunine, J., Combes, M., Bellucci, G., Bibring, J.-P., Capaccioni, F., Cerroni, P., Coradini, A., Formisano, V., Filacchione, G., Langevin, R.Y., McCord, T.B., Mennella, V., Nicholson, P.D., Sicardy, B., 2009. Saturn's Titan: Surface change, ammonia, and implications for atmospheric and tectonic activity. *Icarus* 199, 429–441, doi:10.1016/j.icarus.2008.08.013.
- Paillou, P., Crapeau, M., Elachi, C., Wall, S., Encrenaz, P., 2006. Models of synthetic aperture radar backscattering for bright flows and dark spots on Titan. *J. Geophys. Res.*, 111.
- Paillou, P., Lunine, J., Ruffié, G., Wall, S., Encrenaz, P., Wall, S., Lorenz, R., Janssen, M., 2008. Microwave dielectric constants for Titan-relevant materials. *Geophys. Res. Lett.* 35, L18202.
- Porco, C.C., et al., 2005. Imaging of Titan from the Cassini spacecraft. *Nature* 434, 159–168.
- Quirico, E., Schmitt, B., 1997. Near infrared spectroscopy of simple hydrocarbons and carbon oxides diluted in solid N₂ and as pure ices: implication for Triton and Pluto. *Icarus* 127, 354–378.
- Radebaugh, J., Lorenz, R.D., Kirk, R.L., Lunine, J.I., Stofan, E.R., Lopes, R.M.C., Wall, S.D., The Cassini Radar Team, 2007. Mountains on Titan observed by Cassini Radar. *Icarus* 192, 77–91.
- Rodriguez, S., Le Mouélic, S., Sotin, C., Clénet, H., Clark, R.N., Buratti, B., Brown, R.H., McCord, T.B., Nicholson, D., Baines, K.H., the VIMS Science Team, 2006. Cassini/VIMS hyperspectral observations of the Huygens landing site on Titan. *Planet. Space Sci.* 54, 1510–1523.
- Schmitt, B., Quirico, E., Trotta, F., Grundy, W.M., 1998. Optical properties of ices from the UV to the infrared. In: Schmitt, B., de Bergh, C., Festou, M. (Eds.), *Solar System Ices*. Kluwer Academic Publishers, Dordrecht (Astrophys. Space Sci. Lib., pp. 199–240).
- Shaw, J.H., 1970. Determination of the Earth's surface temperature from remote spectral radiance observations near 2600 cm⁻¹. *Journal of the Atmospheric sciences* 27, 950–959.
- Soderblom, L.A., Kirk, R.L., Lunine, J.I., Anderson, J.A., Baines, K.H., Barnes, J.W., Barrett, J.M., Brown, R.H., Buratti, B.J., Clark, R.N., Cruikshank, D.P., Elachi, Ch., Janssen, M.A., Jaumann, R., Karkoschka, E., Le Mouélic, S., Lopes, R.M., Lorenz, R.D., McCord, T.B., Nicholson, Ph.D., Radebaugh, J., Rizk, B., Sotin, C., Stofan, E.R., Sucharski, T.L., Tomasko, M.G., Wall, S.D., 2007a. Correlations between Cassini VIMS spectra and RADAR SAR images: Implications for Titan's surface composition and the character of the Huygens Probe Landing Site. *Planet. Space Sci.* 55 (13), 2025–2036.
- Soderblom, L., et al., 2007b. Topography and geomorphology of the Huygens landing site on Titan. *Planet. Space Sci.* 55, 2015–2024.
- Sotin, C., et al., 2005. Release of volatiles from a possible cryovolcano from near-infrared imaging of Titan. *Nature* 435, 768–789.
- Stofan, E.R., et al., 2006. Mapping of Titan: results from the first Titan radar passes. *Icarus* 185, 443–456.
- Tobie, G., Lunine, J.I., Sotin, C., 2006. Episodic outgassing as the origin of atmospheric methane on Titan. *Nature* 440, 61–64.
- Tomasko, M.G., Archinal, B., Becker, T., Bézard, B., Bushroo, M., Combes, M., Cook, D., Coustenis, A., de Bergh, C., Dafoe, L.E., Doose, L., Douté, S., Eibl, A., Engel, S., Gliem, F., Grieger, B., Holso, K., Howington-Kraus, E., Karkoschka, E., Keller, H.U., Kirk, R., Kramm, R., Küppers, M., Lanagan, P., Lellouch, E., Lemmon, M., Lunine, J., McFarlane, E., Moores, J., Prout, G.M., Rizk, B., Rosiek, M., Rueffer, P., Schröder, S.E., Schmitt, B., See, C., Smith, P., Soderblom, L., Thomas, N., West, R., 2005. Rain, winds and haze during the Huygens probe's descent to Titan's surface. *Nature* 438 (7069), 765–778.
- Wall, S.D., Lopes, R.M., Stofan, E.R., Wood, C.A., Radebaugh, J.L., Hörst, S.M., Stiles, B.W., Nelson, R.M., Kamp, L.W., Janssen, M.A., Lorenz, R.D., Lunine, J.I., Farr, T.G., Mitri, G., Paillou, P., Paganelli, F., Mitchell, K.L., 2009. Cassini RADAR images at Hotei Arcus and western Xanadu, Titan: Evidence for geologically recent cryovolcanic activity. *Geophys. Res. Lett.* 36, L04203, doi:10.1029/2008GL036415.